The influence of nZVI composites as immobilizing agents on the bioavailability of heavy metals and plant growth in mining metal-contaminated soil

Mohammed Awad Mousa*, Abdullah S. F. Al-Farraj, Mohammad I. Al-Wabel, Hesham M. Ibrahim, Adel R. A. Usman, Hamed A. Al-Swadi, Munir Ahmad* and Mohammad Imran Rafique
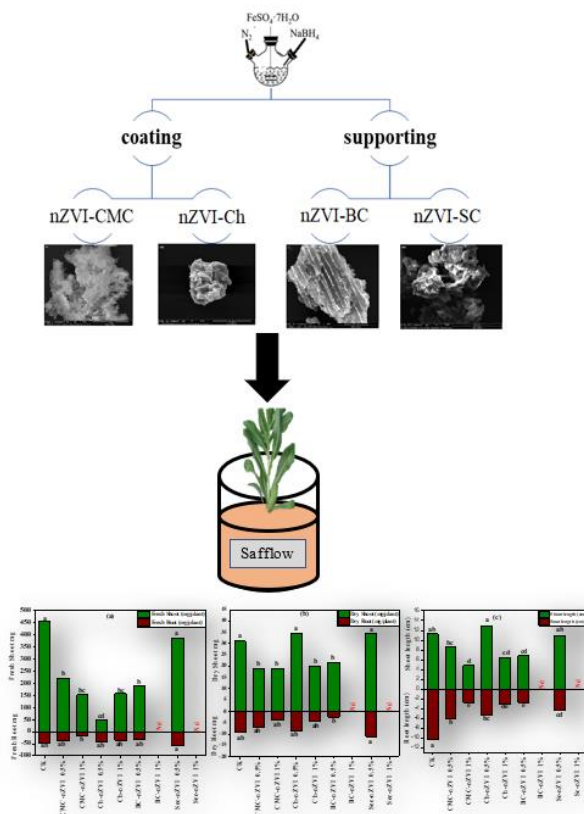
Department of Soil Science, College of Food and Agricultural Sciences, King Saud University, P.O. Box 2460, Riyadh, 11451, Saudi Arabia
*to whom all correspondence should be addressed: e-mail: 441106289@student.ksu.edu.sa, amunir@ksu.edu.sa

Graphical abstract

Abstract

Under the greenhouse scale, nano zero valent iron (nZVI) have been evaluated evaluated by formulation with carboxymethyl cellulose (CMC-nZVI), chitosan (Ch-nZVI), biochar (BC-nZVI), and smectite (SC-nZVI) at rates of 0 and 0.5 and 1% (w/w). The properties of manufactured compounds and their impact on the soil ecosystem planted with safflower (Carthamus tinctorius L.) as a phytoremediation crop for inorganic contaminants in contaminated mining soils have been measured. After 33 days, growth parameters were recorded in harvested plants and the concentrations of some HMs in plant tissues. Furthermore, pH, EC, soluble Na and available Cd, Cu, Pb and Zn concentrations in the treated soil after harvest were analyzed. Results revealed that Ch-nZVI and SC-nZVI application at 0.5% led to a narrow non-significant increase in the dry biomass and the shoot length compared to the control. On the other hand, the application of CMC-nZVI and BC-nZVI resulted in reduced plant growth. All the applied amendments increased soil pH, EC, and soluble Na contents. The soils treated with synthesized nZVI composites showed a considerable increase (non-significant) in available heavy metals in treated soils compared to control. Application of CMC-nZVI1% resulted in increased shoot copper (Cu) and zinc (Zn) (182% and 114%, respectively, compared to control), while Ch-nZVI, SC-nZVI applied at 1%, and BC-nZVI0 applied at 5% resulted in reduce Cu, Zn, and Pb concentrations in roots by 65.2%, 31.4% and 85.5% in Cu, Zn and Pb respectively as compared to control). The phytoremediation indices showed that the uptake and extraction of HMs by safflower plants weren't significant in decreasing heavy metals in polluted soil and the applied materials disabled the actions of hyperaccumulated plant used. Results showed that these materials didn't have a significant effect on immobilize of HMs in mining soil, while the application of Ch-nZVI, SC-nZVI, and BC-nZVI resulted in disabled hyperaccumulated plant to reducing the uptake of Pb, Cu, and Zn. It could be concluded that the application of synthesized nZVI composites to mining polluted soil might be restricted, mainly due to their negative impacts on soil ecosystem besides their side effects on HMs uptake by test hyperaccumulated crop.

Keywords: nZVI based composite materials, heavy metal, bioavailability, contaminated mining soil, remediation

1. Introduction

Soil pollution with heavy metals (HMs) contaminants adversely affects the properties of soil, the yield of crops, and the health of humans. With the progress in agricultural and industrial development, soil and groundwater resources were polluted with enormous concentrations of HMs exceeding the standard limits. Heavy metals are persistent, non-biodegradable human pollutants that can deteriorate the environment and are hazardous for plants, animals, and humans (Al-Swadi *et al.* 2022). On Earth, natural sources of metalloids and HMs are present; however, anthropogenic activities have significantly increased the amount of HMs in the environment. Mining activity releases various harmful substances, such as liquid and solid waste. According to studies, Cd, Cu, Pb, and Zn are the primary contaminants detected in the soil in mining areas. These contaminants deteriorate the soil and have a negative effect on human health because they accumulate in the edible parts of crops (Jia *et al.* 2018). Therefore, mining soil remediation is of importance to reduce negative effect of toxic potential metals. The various in situ and ex situ techniques have been reported to remediated soil HMs (Yuan *et al.* 2017). Chemical stabilization is a characteristic in situ approach that effectively immobilizes metals by utilizing a variety of adsorbent materials (Mandal *et al.* 2020. The remediation of HMs pollution using adsorbent materials has been the focus of many studies because of their ease of application and high efficiency. Common adsorbents include clay materials, organic matter, biochar, and metal oxides (Mandal *et al.* 2020). nZVI is one of these materials that has drawn the most attention since it is a superior HMs adsorbent. The high surface area, abundance of reactive surface sites, and eco-friendly nature of nZVI have contributed to the high efficiency of nZVI when applied to remediate HMs contaminants from systems of groundwater and soil (Zhang *et al.* 2019). According to Gil-Diaz *et al.* (2017), applying 10%, nZVI boosted Pb, Cr, and Zn immobilization by more than 79%; however, nZVI application did not significantly improve Cd immobilization. For nZVI, the most common support materials include activated carbon, silica, montmorillonite, kaolinite, and biochar. Support materials reduce particle aggregation and increase the efficiency of nZVI in remediation processes (Wang *et al.* 2017). In another study, the adsorption capacity of arsenate and arsenate on nZVI was significantly increased and when nZVI particles were supported on activated carbon (Xu *et al*. 2014). A reverse trend was observed when the investigation was conducted into the occurrence, characterization, measurement, and environmental applications of (nZVI) (Jawed *et al.* 2023). In contras a thorough investigation has been conducted into the occurrence, characterization, measurement, and environmental applications of (nZVI) (Jawed *et al.* 2023). However, just a few papers have briefly discussed nZVI regarding environmental uses, risk, fate, and soil contexts. The majority of research centered on using nZVI chemicals in aquatic settings. For instance, Petosa *et al.* (2010) evaluated the effectiveness of nanoparticles for the

purification of water and looked at the behaviors and toxicity of iron based in aquatic environments, while Lei *et al.* (2018) investigated the aggregations and depositions of nZVI in aquatic environments. The injection of nanoscale zero-valent iron (nZVI) into a saturated soil has demonstrated several beneficial effects, as observed in a study conducted by Němeček *et al.* (2014). The primary focus of the study was the immobilization of Cr(VI) in polluted groundwater, and it was found that the injection of nZVI led to a rapid immobilization of Cr(VI). Studies have reported that the use of nanoscale zero-valent iron (nZVI) supported on different types of materials, such as biochar (BC-nZVI), can serve as a stable adsorbent for the effective removal of various contaminants, including metals, from aqueous solutions (Qian *et al.* 2019). Overall, the findings of the study by Hasan *et al.* (2020) suggest that BC-nZVI is a promising and effective adsorbent for the removal of heavy metals, specifically Cd and Zn, from synthetic stormwater, where the results showed BC-nZVI demonstrated a 43% and 57% improvement in metal removal efficiency for Cd and Zn, respectively. BC has been effectively used to eliminate pollutants from water and soil. Considering the benefits and drawbacks of biochar and nZVI, it is highly possible that the formation of BC-nZVI composite will help to minimize the limitations of both products, and the combined features of nZVI-BC would be enhanced, leading to better remediation efficiency (Yang *et al.* 2018). Natural clay deposits have also supported nZVI during remediation processes (Bhowmick *et al.* 2014).

Though extensive studies of the occurrence, characterization, measurement, and environmental applications of (nZVI) has been carried out in the last few decades (Jawed *et al.* 2023), just a few papers have briefly discussed the using of nZVI in minimizing the potential toxicity of inorganic pollutants in soil ecosystem and the growth of plants. Therefore, this study was aimed to investigate the effects of synthesized nZVI composites (CMC-nZVI, Ch-nZVI, BC-nZVI, and SC-nZVI) on immobilization of soil heavy metals (Cd, Cu, Pb, Zn) and the growth parameters of safflower (*Carthamus tinctorius* L) hyperaccumulator plant.

2. Materials and methods

2.1. Soil sampling and analysis

The polluted samples of soil were collected from the mining region of Mahad AD'Dahab region, Saudi Arabia (23°29′59.88″ N and 40°51′56.72″ E). The soil samples were collected at a 0–30 cm depth and combined to form a composite soil sample. After carefully mixing, all soil samples were air dried, and then the soil samples were sieved using a 2 mm screen. The soil sample was prepared for HMs and routine analyses with three replications. In saturated soil paste, the pH of the soil was determined, and EC was analyzed in its extracts (Aboukila and Norton 2017). The hydrometer method measured the soil texture (Mwendwa 2022). The amount of calcium carbonate ($CaCO_3$) in the soil was ascertained using the calcimeter (Erskine *et al.* 2017). The method described by Mylavarapu *et al.* (2014) for

determining soil organic matter (OM) involved potassium dichromate oxidation. The total concentration of Cd, Cu, Pb, and Zn in the collected samples was determined using the Hossner technique (total) (Hossner 1996). After cooling, the digested solutions were filtered through Whatman 42 filter paper and transferred to a volumetric flask holding 50 mL of deionized water. AB-DTPA extraction method was used to measure the available HMs in the soil (Hosseinpur *et al.* 2015). The concentrations of available and total HMs were measured using an inductively coupled plasma-optical emission spectrometer (ICP-OES: PerkinElmer Optima 4300 DV, USA). The results of the total concentrations of HMs are presented in Table 1. The total amounts of Cd, Cu, Pb, and Zn in the soil were 18.81, 783.23, 329.87, and 3325.02 mg kg^{-1}, respectively. The soil's electrical conductivity value was 1.05 dS m^{-1}, and its pH was slightly alkaline (7.48).

Table 1. Some physiochemical characteristics and heavy metals concentrations of soil collected from Mahad AD'Dahab mining area.

Soil property	Value
Particle size distribution	
Silt, %	26.43
Clay, %	4.94
Sand, %	68.63
Texture	sandy loam
EC	1.05
pH	7.48
Calcium carbonate, %	7.23
Organic matter, %	1.9
Soluble ions meq/L	
Ca^{++}	5
Mg^{++}	3.6
Na^+	1.7
K^+	0.12
Cl^-	7
Total heavy metals content, mg/kg	
Zn	3325.02
Cu	783.23
Cd	18.81
Pb	329.87

2.2. Biochar production and smectite collection

In this research, the biochar was prepared by pyrolysis of conocarpus (Conocarpus species) waste gathered from the campus of King Saud University, Riyadh, Saudi Arabia. Subsequently, the conocarpus waste underwent pyrolysis for three hours at 450°C; the resulting biochar was then ground and sieved through a 100 mesh (Al-Wabel *et al.* 2015), the biochar was grinded and sieved through 60 μm. The clay deposits were rich in smectite (> 85%) and were collected from the Khales region. The collected samples were grounded to pass a 60 μm sieve and subjected to physical (particle size distribution and total surface area).

2.3. Synthesis of nZVI composites

CMC-nZVI was prepared by using a tweaked variation of the procedure presented by Yan *et al.* (2013). Briefly, 2.74 g of FeSO$_4\cdot$7H$_2$O was dissolved in 1100 mL three-neck flask by adding 830 mL of deionized water (DI). The mixture was stirred for 25 minutes while pure nitrogen was

continuously supplied. The CMC solution (1 g/100 mL) was added at a concentration of 0.2%. The CMC-nZVI was made by adding 50 mL of 1.85 g/50 mL of NaBH$_4$ solution dropwise every 5 seconds. After 30 minutes of nitrogen purging, the reaction was resumed, and the resulting suspension was vacuum-filtered and dried at 65 degrees Celsius. The same procedure was repeated for the preparation of Ch-nZVI at the same concentration ratios of nZVI and CMC.

BC-nZVI was synthesized in a chemical reduction; the first steps were followed as outlined before in the preparation of CMC-nZVI. Following 25 minutes of stirring, 0.55 g of biochar was added to the mixture. Then, 50 mL of NaBH$_4$ solution (1.85 g per 50 mL) was prepared to cover the surface of the nZVI particles with biochar. Under nitrogen purging, the reaction was carried out for 30 minutes, and the resulting suspension (BC:nZVI mass ratio of 1:1) was washed with DI water after vacuum filtering, and dried at 70°C. The same procedure was repeated for the Synthesis of SC-nZVI at the same concentration ratios of (BC: nZVI mass ratio = 1:1). According to the pathway following a modified protocol of (Ai *et al.* 2007; Üzüm *et al.* 2009).

2.4. Characterization of the synthesized nZVI composites

The synthesized nZVI composites were characterized for chemical and ultimate analysis. X-ray diffraction (Altima IV, Regaku) was employed to investigate the mineralogy of the materials at 45 kV and 30 mA. Iron nanoparticles were placed in a glass holder and scanned from 20° to 90°. This scan range covered all major species of iron and iron oxides. The scanning rate was set at 2.0°min^{-1}. The Fourier-transform infrared spectroscopy technique (FTIR) was used to determine surface functional groups on the surfaces. Scanning electron microscopy (SEM: FEI, Inspect S50, Netherland) was used to explore the surface morphology. Initially, the samples were coated using nano-gold particles for one min. Thereafter, the samples were examined under an SEM and different images were taken using 30-kV at high vacuum. The Brunauer, Emmett and Teller (BET) method were used to determine the specific surface area and microporosity using nitrogen (**N$_2$**) at 77 K as the sorbate (ASAP 2020, Micromeritics, USA). The elemental composition of the synthesized nZVI composites was determined by CHNS-O elemental analyzer (series II, PerkinElmer, USA). For the elemental analyses, the contents of hydrogen (H), carbon, (C), sulfur (S), and nitrogen (N) were measured using the instrument, whereas the contents of oxygen (O) were computed using Eq. [1]. The contents of C, H, and O were used to estimate the atomic ratios of O/C and H/C. Laser doppler velocimetery (Zetasizer Nano ZS, Malvern, UK) was employed to measure the average hydrodynamic size for the particles of the different nZVI composites.

$$O\ (\%) = 100 - \left[C\ (\%) + H\ (\%) + N\ (\%) + S\ (\%) + ash\ (\%) \right] \qquad \text{Eq. [1]}$$

2.5. Greenhouse experiments

The CMC-nZVI, Ch-nZVI, BC-nZVI, and SC-nZVI composites were added at 0%, 0.5% and 1% (w/w) application rates

and combined with 1 kg contaminated soil. Control was added with no amendment. The amended and unamended (control) soils were filled in wet to 60% of the percentage of soil saturation and stored at room temperature (23±2°C) for 30 days. To guarantee uniformity between the soil and the compounds, it was thoroughly mixed, blending each kilogram of soil separately then agitated. After that, it was moved to the pots to start the greenhouse experiment (Mandal *et al.* 2020). Soil with nZVI composites (CMC-nZVI, Ch-nZVI, BC-nZVI, and SC-nZVI) was evaluated for their ability to immobilize (Cd, Pb, Cu, and Zn) in contaminated soil in a pot greenhouse experiment. Plastic pots with porous bottom were selected and filled with 1 kg contaminated soil. Amendments (nZVI composites) were added at three different rates including 0%, 0.5%, and 1.0% (w/w). A control treatment was also addedwith no added amendment and soil only. Additionally, the soil was fertilized with 0.0625 g/kg of phosphate (P_2O_5), potassium (K_2O), and 0.003 g/kg of nitrogen (N) fertilizers (Ren *et al.* 2021). In each pot 10 seeds of safflower were added, and plant growth was observed regularly to investigate treatment impact on plant growth. Throughout experiment soil moisture in pots was maintained at field capacity and pots were irrigated with tap water to adjust soil moisture level.

2.6. Plant and soil analyses

Plants were harvested after a period of 33 days. To harvest plants pots were flushed with excessive water to carefully extract plant roots and shoots. Harvested plants were shifted to lab and analyzed for growth parameters including plant fresh and dry weight and root and shoot length. Latterly plant roots and shoots were analyzed for heavy metals uptake by digesting plants following Ahmad *et al.* 2019)) method. Additionally, after harvesting soil samples were collected from pots and were extracted by AB-DTPA extract to assess available contents of heavy metals.

2.7. Phytoextraction indices

The bioconcentration factor values (BCF) in shoots and roots were computed as shown in Eq. [2] to check phytoextraction and phytostabilization ability (Zhuang *et al*. 2007):

$$(BCF) = \frac{metal\ concentration\ in\ plant\ shoot\ or\ root}{metal\ concentration\ in\ soil} \qquad \text{Eq. (2)}$$

Additionally, the following method was used to determine translocation factor values (TF) as shown in Eq. [3], which represents the capacity of Safflower plants to move HMs from the roots to the shoots (McGrath and Zhao 2003; Zacchini *et al.* 2009):

$$(TF) = \frac{metal\ concentration\ in\ aerial\ parts}{metal\ concentration\ in\ root} \qquad \text{Eq. (3)}$$

2.7.1. Quality control

Quality control measurements were strictly followed during all experimental activities. High-quality, analytical-grade chemicals were used. In addition, standard procedures for cleaning glassware, testing and calibration of equipment, and measurement accuracy were followed. To ensure quality control and accuracy during the measurement of HMs concentrations, the measurement was repeated three times in 10% of the total number of analyzed soil and leachate samples.

2.7.2. Statistical analysis

SPSS program (version 18, SPSS Inc., Chicago, IL) was applied for statistical analysis of the experimental data (SPSS 2012). The average and standard deviation (±1SD) were applied. The least significant difference (LSD) test at a 5% level of significance was used to evaluate the comparison between averages of treatments.

3. Results and discussion

3.1. Characterizations of nZVI composites

Figure 1 displays the results of the XRD pattern for CMC-nZVI, Ch-nZVI, BC-nZVI, and SC-nZVI. The CMC-nZVI composite's diffraction peaks revealed the presence of nZVI at 2θ = 44.8° and 65.6° as well as Fe_2O_3 at 2θ = 30.9°. In our results, Fe_2O_3 diffraction peak was much less intense demonstrating that CMC minimized the oxidation of Fe0 during the preparation process as shown in Figure 1. (Ibrahim *et al.* 2019). Furthermore, the CMC-nZVI composites particles appear to have been small crystallites as can be seen with large diffraction peak (Zhao *et al.* 2019). The XRD pattern of Ch-nZVI revealed considerably nosier baseline diffraction peaks, suggesting amorphous structure (Chen *et al.* 2019). Li *et al.* (2017) reported that diffraction peak at 2θ = 24.3° in the BC-nZVI composites could be due to the presence of carbon. According to Unsoy *et al.* (2012), the presence of chitosan could be responsible for the sharp peak at 2θ = 17.2°, and Fe0 was linked to the diffraction peak at 2θ = 44.9°. Furthermore, it was observed that the absence of the diffraction peaks for FeO(OH) and Fe_2O_3 in the synthesized Ch-nZVI could be due to the reason that the addition of chitosan reduced the oxidation of Fe^0. According to earlier studies (Zou *et al*. 2016; Jin *et al.* 2016), chitosan can function as a stabilizer during the synthesis of a Ch-nZVI composite. The findings show that during the synthesis of the BC-nZVI composite, the oxidation of nZVI nanoparticles was more noticeable on biochar surfaces. These outcomes agree with earlier research by Chen *et al.* (2019). The additional functional groups that contain oxygen (such as carboxyl, hydroxyl, aliphatic, etc.) on the surfaces of BC may be responsible for the increased oxidization of Fe0 during the preparation of BC-nZVI composite. These groups speed up the formation of oxygen-containing complexes with Fe0, increasing the formation of iron oxide and hydroxide (Lin *et al.* 2010). According to Deon *et al.* (2022), the XRD pattern of the SC-nZVI composite revealed some diffraction peaks that suggested the presence of smectite (2θ = 6.2° and 36.1°), quartz (2θ = 26°), and Fe^0 (2θ = 44.9°). The BC-nZVI composite revealed extra diffraction peaks at 2θ = 20.3°, 31.1°, and 44.9°, which corresponded to FeO(OH), Fe_2O_3, and Fe0, respectively, in contrast to the XRD patterns of the Ch-nZVI. These findings show that during the synthesis

of the SC-nZVI composite, nZVI particles were successfully loaded onto the surfaces of the SC.
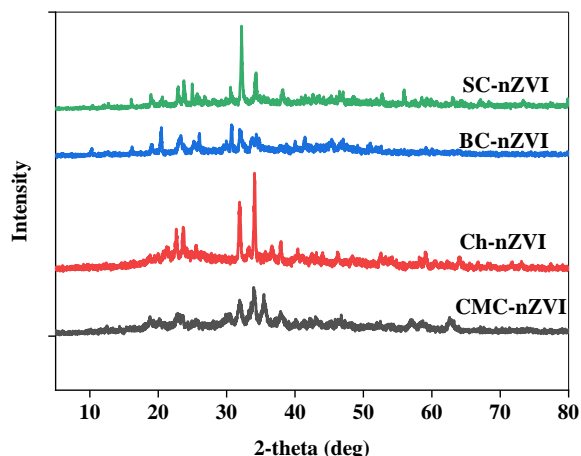

Figure 1. X-ray diffraction patterns (XRD) of nano-zero valent iron (nZVI) composites with carboxy-methylcellulose (CMC-nZVI), chitosan (Ch-nZVI), biochar (BC-nZVI), and smectite (SC-nZVI)
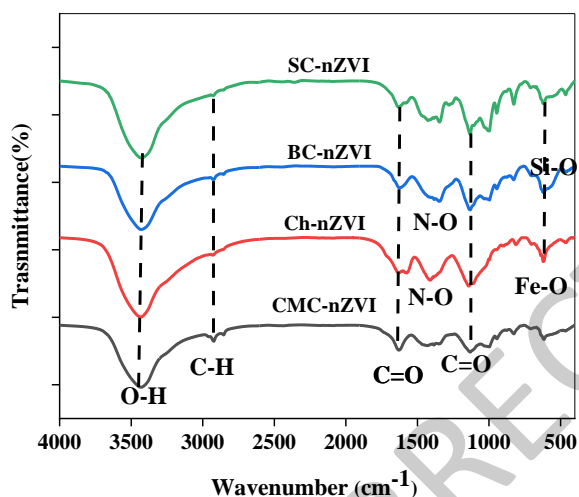

Figure 2. FTIR spectra of nano-zero valent iron (nZVI) composites with carboxy-methylcellulose (CMC-nZVI), chitosan (Ch-nZVI), biochar (BC-nZVI), and smectite (SC-nZVI)

FTIR spectra in the 400–4000 cm^{-1} wavenumber region was used to examine the surface functional groups of nZVI composites (Figure 2). When biochar and chitosan were successfully loaded onto the surfaces of nZVI during the preparation of BC-nZVI and Ch-nZVI composites, a new characteristic peak at 1360 and 1410 cm^{-1} belonging to the stretching vibration of N–O was observed for the BC-nZVI and Ch-nZVI composites. In comparison to the pristine BC, the stretching vibrations O-H in the BC-nZVI and Ch-nZVI composites were much greater, two peaks were also visible in the FTIR spectra, at 1623 and 2923 cm^{-1}, respectively. The generated nZVI composites morphological structure was assessed with (SEM), (Figure. 3) displayed the SEM analyses of the CMC-nZVI, Ch-nZVI, BC-nZVI, and SC-nZVI composites. Ch-nZVI was randomly distributed in the agglomerated formation, while the crystalline on the surface of CMC-nZVI was observed.

The results of FTIR spectra showed distinct bands responsible for various functional groups. O-H vibration stretching is generally responsible for the broad band observed in the FTIR spectra at 3430 cm-1 (Chen *et al.* 2019) corresponding to the aliphatic (C-H) and aromatic rings (C=C) molecules (Lin *et al.* 2020). According to Li *et al.* (2012), the SC-nZVI composite had a peak at 457 cm-1, which is associated with the presence of Si-O. The distinctive peak between 680 and 685 cm-1 could be related to the nZVI and the Fe–O stretching vibration, respectively, which was clearly visible in all the nZVI composites. This indicates that the nZVI had been successfully loaded onto the surfaces of the support materials (CMC, BC, Ch, and SC) (Shu *et al.* 2020; Wei *et al.* 2020). The characteristic peak of C=O was shifted from 1441 cm-1 in pristine BC to 1100 cm-1 in the nZVI composites, which could be due to the attachment of the nZVI particles with the supportive materials (Li *et al.* 2012; Zhu *et al.* 2018). Chen *et al* (2019) suggested that the adsorbed water and chitosan molecules in both BC-nZVI and Ch-nZVI composites contributed to the increased number of O-H groups. Because CMC can negatively charge the surfaces of nZVI particles, which greatly increases the electrostatic repulsion between the nanoparticles. On the other hand, nZVI surface modification with CMC led to a decrease in aggregation and a more even dispersion of CMC-nZVI (Karabelli *et al.* 2008). The SEM images demonstrated that BC-nZVI had smaller and more scattered particles, while SC-nZVI surfaces were amorphous, porous, uneven, and rough. Layering of nZVI was observed on the surface of BC, which may offer a rougher surface and more reactive surface area for Cd, Cu, Pb, and Zn sorption. The volatilization of organic components resulted in porous surfaces on the surface structures of the BC-nZVI samples. Deep channels and pores in BC-nZVI started to show more clearly. On the surface of the BC, pores might still be accessible for the adsorption of Cd, Cu, Pb, and Zn (Premarathna *et al.* 2019).
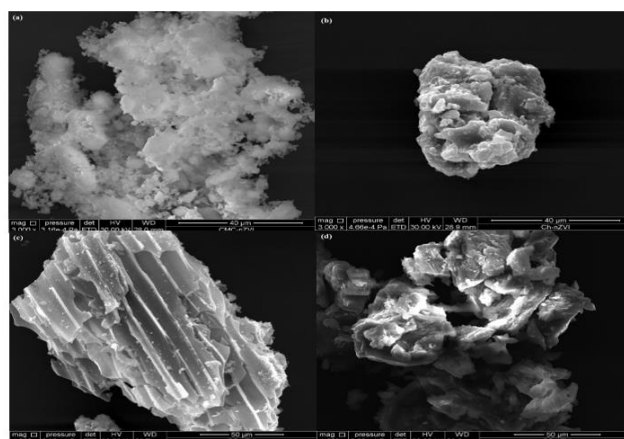

Figure 3. Scanning electron microscope images of the nano-zero valent iron (nZVI) composites with (a) carboxy-methylcellulose (CMC-nZVI), (b) chitosan (Ch-nZVI), (c) biochar (BC-nZVI), and (d) smectite (SC-nZVI)

Table 2. Chemical, elemental composition, surface properties, average hydrodynamic size, and zeta potential of the nano-zero valent iron (nZVI) composites with carboxy-methylcellulose (CMC-nZVI), chitosan (Ch-nZVI), biochar (BC-nZVI), and smectite (SC-nZVI)

Parameter	Unit	CMC-nZVI	Ch-nZVI	BC-nZVI	SC-nZVI
pH	-	8.54	5.15	4.27	8.75
C	%	10.804	16.393	14.681	1.494
H	%	2.468	3.011	1.281	1.348
N	%	-	7.699	5.124	-
S	%	2.882	2.32	2.393	1.034
O	%	83.846	70.577	76.521	96.124
O/C	%	5.820	3.229	3.909	48.255
H/C	%	2.741	2.204	1.047	10.827
Surface area	$m^2\ g^{-1}$	19.61	13.55	117.84	36.19
Total volume in pores	$cm^3\ g^{-1}$	0.0237	0.0196	0.1849	0.0466
Pore size	Å	48.34	57.85	62.76	51.5
Zeta potential	mV	-20.11	-17.58	-12.61	-9.52

Table 3. Treatment impacts on soil pH, electrical conductivity (EC), and soluble Na

Treatments	pH	EC dS m^{-1}	Na (mg kg^{-1})
CK	7.52 de	0.62 g	14.1 h
CMC-nZVI 0.5%	7.64 cd	0.98 f	37.3 f
CMC-nZVI 1%	7.91 b	1.17 c	57.3 c
Ch-nZVI 0.5%	7.61 e	1.06 d	36.8 f
Ch-nZVI 1%	7.83 b	1.02 e	44.1 d
BC-nZVI 0.5%	7.71 c	1.08 d	40.9 e
BC-nZVI 1%	8.01 a	1.21 b	60.9 b
SC-nZVI 0.5%	7.83 b	1.23 b	33.9 g
SC-nZVI 1%	7.95 b	1.29 a	63.3 a
LSD at p =0.05	0.12	0.03	2.12

nZVI: nano-zero valent iron; CMC-nZVI: stabilized nZVI composites with carboxy-methylcellulose, Ch-nZVI: stabilized nZVI composites with chitosan, BC-nZVI: stabilized nZVI composites with biochar, and SC-nZVI: stabilized nZVI composites with smectite

Analysis of the elemental composition of the nZVI compounds revealed that the content of carbon (C) decreased significantly from 85.7% in pristine BC to 10.8, 16.3, 14.6, and 1.4% in the CMC-nZVI, Ch-nZVI, BC-nZVI, and SC-nZVI composites, respectively. In contrast, the content of oxygen (O) increased significantly from 7.7% in pristine BC to 83.8, 70.6, 76.5, and 96.1% in the CMC-nZVI, Ch-nZVI, BC-nZVI, and SC-nZVI composites, respectively. the higher O contents in the nZVI composites could be attributed to the formation of additional surface functional groups and iron oxide/hydroxide compounds (Wang *et al.* 2017). The content of nitrogen (N) reached 7.7 and 5.1% in the Ch-nZVI and BC-nZVI, respectively, whereas the content of N was almost not detectable in both CMC-nZVI and SC-nZVI composites. The content of sulfur (S) ranged between 1-3% for all composites (Table 2). On the other hand, the pore size of the nZVI decreased from 68.52 Å to 48.34, 57.85, and 51.50 Å in the CMC-nZVI, Ch-nZVI, and SC-nZVI composites, respectively. These results suggested that the modification of nZVI using the stabilizing (CMC and chitosan) and supporting (BC and SC) materials profoundly altered the surface properties of nZVI, reduced aggregation, and increased the specific surface area of the synthesized nZVI composites (Chen *et al.* 2019; Zhang *et al.* 2019). The BET surface area, pore volume, and pore size of the different nZVI composites were determined using N_2 adsorption/desorption isotherms at 77 K (Table 2). For the nZVI composites, the BC-nZVI composite showed a decrease in the specific surface area from 330 to 117 $m^2\ g^{-1}$, and an increase in pore volume and pore size to 0.1849 cm3 g^{-1} and 62.76 A°, respectively.

3.2. Impacts of stabilized nZVI composites on available heavy metals

The results demonstrated that the soil additions had a considerable impact on the soil's pH, EC, and soluble Na (Table 3). Compared to control, application of soil additives increased soil pH by 0.12, 0.39, 0.09, 0.31, 0.19, 0.49, 0.31, and 0.43 unit for CMC-nZVI at 0.5%, CMC-nZVI at 1%, Ch-nZVI at 0.5%, Ch-nZVI at 1%, BC-nZVI at 0.5%, BC-nZVI at 1%, SC-nZVI at 0.5%, and SC-nZVI at 1%, respectively. Likewise, the addition of soil additives increased soil EC by 0.36, 0.55, 0.44, 0.40, 0.46, 0.59, 0.61, and 0.67 dS m^{-1} for CMC-nZVI at 0.5%, CMC-nZVI at 1%, Ch-nZVI at 0.5%, Ch-nZVI at 1%, BC-nZVI at 0.5%, BC-nZVI at 1%, SC-nZVI at 0.5%, and SC-nZVI at 1%, respectively, compared to control. The addition of soil additives increased soil soluble Na by 164.54%, 306.38%, 160.99%, 212.77%, 190.07, 331.91%, 140.43%, and 348.94% for CMC-nZVI at 0.5%, CMC-nZVI at 1%, Ch-nZVI at 0.5%, Ch-nZVI at 1%, BC-nZVI at 0.5%, BC-nZVI at 1%, SC-nZVI at 0.5%, and SC-nZVI at 1%, respectively, compared to control. The highest salinity and/or sodium increase was pronounced for SC-nZVI at 1%, followed by BC-nZVI at 1% and CMC-nZVI at 1%.

The results of the available concentration of HMs, which were extracted by AB-DTPA demonstrated that the

highest concentration was Zn (408.93–522.20 mg/kg), followed by Cu (95.86–113.85 mg/kg), Pb (48.06–62.66 mg/kg), and Cd (1.23–1.70 mg/kg) However, Cd and Pb concentrations were all below the threshold values (EU/UK/USEPA threshold) for the heavy metal in soil (Adesuyi *et al.* 2015) (Table 4). Our findings demonstrated that, depending on the kind of nZVI composites utilized,

the additives substantially impacted the amounts of soil metals. In relation to potential metal extraction from AB-DTPA, the current investigation of soils treated with CMC-nZVI at 1% and Ch-nZVI at 1% showed considerable increases or no significant effect when compared to control.

Table 4. Impacts of stabilized nano-zero valent iron (nZVI) composites with carboxy-methylcellulose (CMC-nZVI), chitosan (Ch-nZVI), biochar (BC-nZVI) biochar, and smectite (SC-nZVI) on the availability of heavy metals in soil (mg/kg)

Treatments	AB-DTPA extractable HMs			
	Cd	Cu	Pb	Zn
CK	1.23 b	95.85 b	49.90 de	431.27 cd
CMC-nZVI 0.5%	1.48 ab	102.81 ab	56.77 abc	477.73 abc
CMC-nZVI 1%	1.70 a	113.17 a	62.66 a	522.20 a
Ch-nZVI 0.5%	1.38 b	104.94 ab	58.80 ab	476.47 abc
Ch-nZVI 1%	1.37 b	113.15 a	60.41 ab	501.73 ab
BC-nZVI 0.5%	1.25 b	100.73 ab	50.98 cde	420.66 cd
BC-nZVI 1%	1.24 b	94.74 b	48.06 e	408.93 d
SC-nZVI 0.5%	1.41 ab	102.87 ab	55.45 bcd	460.37 bcd
SC-nZVI1%	1.38 b	105.34 ab	54.52 bcde	448.60 bcd
LSD at p = 0.05	0.29	14.82	6.86	58.48

CK: control; CMC-nZVI at 0.5% and 1%: Carboxy-methylcellulose with nZVI at dosage at 0.5 and 1 % respectively; Ch-nZVI at 0.5% and 1%: Chitosan with nZVI at dosage at 0.5 and 1 % respectively; BC-nZVI at 0.5% and 1%: biochar with nZVI at dosage at 0.5 and 1 % respectively; SC-nZVI at 0.5% and 1%: smectite with nZVI at dosage at 0.5 and 1 % respectively; LSD: Different letters indicate significant differences.
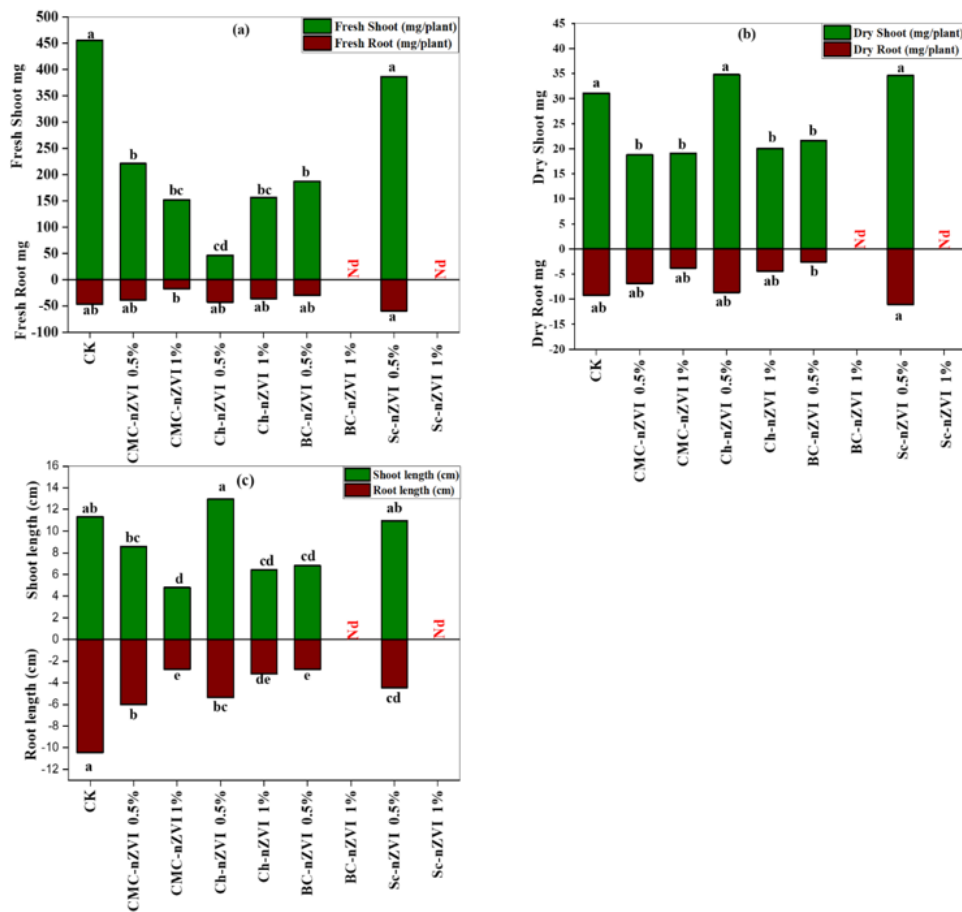

Figure 4. (a) Fresh weight of shoots and roots of plants; (b) dry weight of shoots and roots of plants; (c) length of plant shoots and roots as affected by stabilized nano-zero valent (nZVI) composites with carboxy-methylcellulose (CMC-nZVI 0.5%, CMC-nZVI 1%), chitosan (Ch-nZVI 0.5%, Ch-nZVI 1%), biochar (BC-nZVI 0.5%, BC-nZVI 1%), smectite (SC-nZVI 0.5%, and SC-nZVI 1%) respectively)

3.3. Impacts of stabilized nZVI composites on plant growth

Figure 4 shows the impact of a treatment on the fresh weights and dry weights of the roots and shoots of a safflower plant's growth in a pot experiment. The results showed that SC-nZVI at 1% and BC-nZVI at 1% inhibited seed germination, but no plant grew in both treatments. Additionally, most other treatments significantly decreased the biomass weight of plant shoots and plant length. For example, com-pared to the control, the addition of CMC-nZVI 0.5%, CMC-nZVI 1%, Ch-nZVI 0.5%, Ch-nZVI 1%, BC-nZVI 0.5%, BC-nZVI 1%, SC-nZVI 0.5%, and SC-nZVI 1% resulted in approximately 51.5%, 66.7%, 89%, 65.7%, 59%, 100%, 15.2%, and 100% decreases in the fresh weight of shoots, respectively. Meanwhile, com-pared to the control, the addition of CMC-nZVI 0.5%, CMC-nZVI 1%, Ch-nZVI 0.5%, Ch-nZVI 1%, BC-nZVI 0.5%, BC-nZVI 1%, SC-nZVI 0.5%, and SC-nZVI 1% resulted in approximately 39.6%, 38.6%, 11.9%, 35.5%, 30.4%, 100%, 11.4%, and 100% decreases in the dry weight of shoots, respectively. Research in this field has shown that nZVI has distinct biological impacts on the growth and development of plants, emphasizing the fact that nZVI has strong dosage inhibition at low doses and negative excitatory effects at higher doses (Cui *et al.* 2023; Baragano *et al.* 2022; Yang *et al.* 2022). Yang *et al.* (2023), found that (nZVI) generates negative effects on the growth of maize, acting as hazardous. According to our findings, the additions raised the concentrations of soluble sodi-um and soil salinity, which may have contributed to the detrimental impacts of the additives containing nanoscale zero-valent iron on plant growth. The correlation study showed that there is a significant

negative correlation between plant growth parameters (biomass weight or plant length) and soil properties (pH, EC, or soluble Na). A mediated decrease in nitrogen uptake may be the cause of the decrease in plant dry matter (Pradas-del-Real *et al.* 2013), or the distortion of the structure of plant roots, which subsequently strained the plants' ability to absorb nutrients and grow vigorously (Ali *et al.* 2013; Gill *et al.* 2014). The nature of the materials and the type of soil employed in this study most likely contributed to the distortion of the plant roots' structure (Rajkovich *et al.* 2012).

3.4. Treatment impacts of HMs concentration and uptake in plants

Table 5 shows the HMs concentrations in plant shoots and roots. The results showed that shoot Cd and Pb, as well as root Cd concentrations, were under the detection limit of ICP. The Cu and Zn concentrations in shoots significantly increased by 182 and 114% in plants treated with CMC-nZVI, respectively, by 1% compared to the control. On the contrary, compared to the control, the Cu concentrations in roots significantly decreased by 65.2% in plants treated with Ch-nZVI 1%. Similarly, adding Ch-nZVI 1% and BC-nZVI 0.5% significantly reduced root Zn concentrations by 31.4 and 27.4%, respectively. Adding CMC-nZVI 0.5% and BC-nZVI 0.5% significantly decreased Pb concentrations by 47.9 and 85.5% compared to control, respectively. Additionally, both CMC-nZVI 1% and Ch-nZVI 1% decreased root Pb concentration from 89.46 mg/kg to under the detection limit (UDL) of ICP. It was observed that the concentrations of HMs in shoots were below the permissible limit, suggested lower translocation of HMs from roots to shoots (Gupta *et al.* 2006).

Table 5. Concentrations of heavy metals in plant shoots and roots as affected by stabilized nano-zero valent iron (nZVI) composites with carboxy-methylcellulose (CMC-nZVI), chitosan (Ch-nZVI), biochar (BC-nZVI) biochar, and smectite (SC-nZVI).

	Shoot concentrations (mg/kg)				Root concentrations (mg/kg)			
	Cd	Cu	Pb	Zn	Cd	Cu	Pb	Zn
CK	UDL	27.24 b	UDL	239.86 b	UDL	485.94 a	89.46 a	2647.64 a
CMC-nZVI 0.5%	UDL	35.63 ab	UDL	283.42 b	UDL	479.29 a	46.60b	2647.49 a
CMC-nZVI 1%	UDL	76.94 a	UDL	512.35 a	UDL	355.89 ab	UDL	2525.38 ab
Ch-nZVI 0.5%	UDL	43.07 ab	UDL	383.61 ab	UDL	482.50 a	113.54 a	2722.25 a
Ch-nZVI 1%	UDL	30.79 b	UDL	342.37 ab	UDL	168.99 b	UDL	1816.37 c
BC-nZVI 0.5%	UDL	47.81 ab	UDL	367.94 ab	UDL	331.61ab	12.95 bc	1920.98 bc
BC-nZVI 1%	Nd	Nd	Nd	Nd	Nd	Nd	Nd	Nd
SC-nZVI 0.5%	UDL	17.82 b	UDL	286.94 b	UDL	355.44 ab	118.48 a	2324.26 abc
SC-nZVI 1%	Nd	Nd	Nd	Nd	Nd	Nd	Nd	Nd
LSD at p = 0.05	–	44.90	–	216.83	–	206.43	39.14	638.17

CK: control; CMC-nZVI 0.5% and 1%: Carboxy-methylcellulose with nZVI at dosage 0.5 and 1 % respectively; Ch-nZVI 0.5% and 1%: Chitosan with nZVI at dosage 0.5 and 1 % respectively; BC-nZVI 0.5% and 1%: biochar with nZVI at dosage 0.5 and 1 % respectively; SC-nZVI 0.5% and 1%: smectite with nZVI at dosage 0.5 and 1 % respectively; UDL: under detection limit; Nd: no plants; LSD: Different letters indicate significant differences.

Table 6 shows that HMs uptake to shoot and root significantly ($p < 0.05$) increased with the Ch-nZVI at 0.5% and SC-nZVI at 0.5% application compared to the control. Application rate of 0.5% for Ch-nZVI and SC-nZVI increased the shoot uptake of Cu by 81.3% and 17.3%, and Zn by 80.9% and 34.1%, respectively, compared to the control, while showing no significant differences compared to the control. The levels of Cd and Pb in shoots were generally low, ranging from zero mg/kg in many plants to UDL in

others, and well below the EU, UK, and USEPA thresholds for heavy metals in plants, the parameters were provided by the (EU/UK/USEPA threshold) (Adesuyi *et al.* 2015).

Table 7 displays the phytoextraction indices that were computed for this investigation. The TF is calculated as the ratio metal concentration in the shoots and the roots. It is used to indicate the transfer of metal from the roots to the shoots. While the BCF value indicates the metal

concentration in the shoot to that in the soil. Our results exhibited that TF was <1 in all treatments, suggesting that the absorbed concentrations of Cu, Pb, and Zn accumulated in plants roots, and did not translocate to the shoots. Our finding demonstrated that there was no transfer of Pb from roots to shoots. The higher TF values in all amended soil showed a greater translocation of Cu and Zn from plant roots toward plant shoots. In comparison with the control, CMC-nZVI 1% and Ch-nZVI 1% showed a higher translocation of Cu and Zn from roots to shoots, respectively. On the other hand, a 100% reduction in TF values was observed for Cd and Pb after application of all the amendments. According to previous study by Usman *et al.* (2013) and Lu *et al.* (2014), phytoextraction indices for plant species such as TF and BCF with values larger than unity are typically considered to be hyperaccumulators, while TF and BCF values less than unity are typically considered to be excluders. Plants with TF > 1 are classified as hyperaccumulators, and those with TF < 1 are called excluders (Usman and Mohammed 2009). Overall, application of the amendments increased the phytoremediation indices; however, the increments were below unity, suggesting unsuitability as hyperaccumulators for practical application.

Table 6. Uptake of heavy metals by the plant shoots and roots as affected by stabilized nano-zero valent iron (nZVI) composites with carboxy-methylcellulose (CMC-nZVI), chitosan (Ch-nZVI), biochar (BC-nZVI) biochar, and smectite (SC-nZVI)

Treatment	uptake of Cd (ug/plant^{-1})	uptake of Cu (ug/plant^{-1})	uptake of Pb (ug/plant^{-1})	uptake of Zn (ug/plant^{-1})
		uptake by shoots		
CK	UDL	0.8567 ab	UDL	7.4833 b
CMC-nZVI 0.5%	UDL	0.6483 ab	UDL	5.1342 bc
CMC-nZVI 1%	UDL	1.4117 a	UDL	9.5131 ab
Ch-nZVI 0.5%	UDL	1.5542 a	UDL	13.5375 a
Ch-nZVI 1%	UDL	0.6139 ab	UDL	6.8264 b
BC-nZVI 0.5%	UDL	0.7911 ab	UDL	8.0256 ab
BC-nZVI 1%	Nd	Nd	Nd	Nd
SC-nZVI 0.5%	UDL	0.9572 b	UDL	10.0389 ab
SC-nZVI 1%	Nd	Nd	Nd	Nd
		uptake by Roots		
CK	UDL	4.5567 ab	0.9067 a	24.6267 ab
CMC-nZVI 0.5%	UDL	3.3050 abc	0.3542 a	18.4233 abc
CMC-nZVI 1%	UDL	1.3764 abc	UDL	9.6078 abc
Ch-nZVI 0.5%	UDL	4.3889 bc	0.8167 a	25.1069 ab
Ch-nZVI 1%	UDL	0.8097 bc	UDL	8.1403 bc
BC-nZVI 0.5%	UDL	0.8533 bc	0.0333 a	4.9433 c
BC-nZVI 1%	Nd	Nd	Nd	Nd
SC-nZVI 0.5%	UDL	5.0917 a	0.8333 a	28.3000 c
SC-nZVI 1%	Nd	Nd	Nd	Nd

CK: control; CMC-nZVI 0.5% and 1%: Carboxy-methylcellulose with nZVI at dosage of 0.5 and 1 % respectively; Ch-nZVI at 0.5% and 1%: Chitosan with nZVI at dosage of 0.5 and 1 % respectively; BC-nZVI at 0.5% and 1%: biochar with nZVI at dosage of 0.5 and 1 % respectively; SC-nZVI at 0.5% and 1%: smectite with nZVI at dosage of 0.5 and 1 % respectively; UDL: under detection limit; Nd: no plant.

Table 7. Treatment effects on the shoot-to-root ratio, bioconcentration factor values (BCF) and the adsorbed metal by the adsorbed shoots/metal of the entire plant (%)

Treatment	CK	CMC-nZVI 0.5%	CMC-nZVI 1%	Ch-nZVI 0.5%	Ch-nZVI 1%	BC-nZVI 0.5%	BC-nZVI 1%	SC-nZVI 0.5%	SC-nZVI 1%
				Shoot-to-root ratio (TF)					
Cd	0	0	0	0	0	0	Nd	0	Nd
Cu	0.056 bc	0.074 bc	0.212 ab	0.085 bc	0.397 a	0.053 bc	Nd	0.063 bc	Nd
Pb	0	0	0	0	0	0	Nd	0	Nd
Zn	0.091 bc	0.106 ab	0.199 a	0.139 ab	0.195 a	0.066 bc	Nd	0.130 ab	Nd
				Bioconcentration factor values Shoot (BCF)					
Cd	0	0	0	0	0	0	Nd	0	Nd
Cu	0.035 bc	0.045 abc	0.098 a	0.055 ab	0.039 bc	0.041 bc	Nd	0.023 bc	Nd
Pb	0	0	0	0	0	0	Nd	0	Nd
Zn	0.072 b	0.085 b	0.154 a	0.115 ab	0.103 ab	0.111 ab	Nd	0.086 b	Nd
				Bioconcentration factor values Root (BCF)					
Cd	0	0	0	0	0	0	Nd	0	Nd
Cu	0.620 a	0.612 a	0.454 ab	0.616 a	0.216 bc	0.141 c	Nd	0.454 ab	Nd
Pb	0.796 ab	0.796 ab	0.760 ab	0.819 a	0.546 b	0.193 c	Nd	0.699 ab	Nd
Zn	0.271 a	0.141 ab	0.000	0.229 a	0.000	0.013 b	Nd	0.120 ab	Nd

nZVI: nano-zero valent iron; CMC-nZVI: stabilized nZVI composites with carboxy-methylcellulose, Ch-nZVI: stabilized nZVI composites with chitosan, BC-nZVI: stabilized nZVI composites with biochar, and SC-nZVI: stabilized nZVI composites with smectite.

4. Conclusion

In this work, nanoscale zero-valent iron (nZVI) through synthesis with CMC (CMC-nZVI), chitosan (Ch-nZVI), biochar (BC-nZVI), and smectite (SC-nZVI) were applied in polluted soils cultivated with safflower were evaluated in minimizing the risks of heavy metals in mining soils. The results showed that nZVI compounds significantly increased soil pH, EC, and soluble Na. Also, the applied materials had no significant effect on reducing the contents of HMs in the aboveground biomass of safflower plants. However, the application of Ch-nZVI, BC-nZVI, or SC-nZVI had no significant effect and led to a decrease in the concentration of heavy metals in the rhizosphere, especially for Pb, Cu, and Zn as well as a narrow but non-significant increase in plant weight. The applied modifications were not feasible for the immobilization of HMs or extraction by safflower plants. Due to the negative effects of composite materials, it can be concluded that the application of nZVI composites to soil may be limited and can only be used in aquatic environments.

Acknowledgments

Author Contributions

MAM and ARU conceptualized the project, developed methodology, and written the draft, ASA supervised the project, MIA acquired funding and managed resources, HMI validated the results, ARU collected soil samples, HAA conducted the analyses, MA helped in lab investigation, MIR help conduct the analyses, whereas ASA, MIA, HAA, MA, and MIR reviewed and edited the manuscript.

Conflicts of Interest

The authors declare that there is no conflict of interest.

References

Aboukila E.F. and Norton J.B. (2017). Estimation of saturated soil paste salinity from soil-water extracts, *Soil Science*, **182**(3), 107–113.

Adesuyi A.A., Njoku K.L. and Akinola M.O. (2015). Assessment of heavy metals pollution in soils and vegetation around selected industries in Lagos State, Nigeria. *Journal of Geoscience and Environment Protection*, **3**(7), 11–19.

Ahmad M., Al-Swadi H.A., Ahmad J., Usama M., Mousa M.A., Lubis N.M. and Al-Farraj A.S. (2023). Silica-embedded nutrient-doped biochar improves nutrient availability and safflower (Carthamus tinctorius L.) growth in cadmium-and lead-contaminated soil, *Journal of Soils and Sediments*, **25**, 1–15.

Ahmad M., Usman A.R., Al-Faraj A.S. Ahmad M., Sallam A. and Al-Wabel M.I. (2018). Phosphorus-loaded biochar changes soil heavy metals availability and uptake potential of maize (Zea mays L.) plants. *Chemosphere*, **194**, 327–339.

Ahmadi M., Foladivanda M., Jaafarzadeh N., Ramezani Z., Ramavandi B., Jorfi S. and Kakavandi B. (2017). Synthesis of chitosan zero-valent iron nanoparticles-supported for

cadmium removal: characterization, optimization and modeling approach, *Journal of Water Supply: Research and Technology Aqua*, **66**(2), 116–130.

Ai Z., Lu L., Li J., Zhang L., Qiu J. and Wu M. (2007). Fe@ Fe2O3 core shell nanowires as iron reagent. 1. Efficient degradation of rhodamine B by a novel sono-Fenton process, *The Journal of Physical Chemistry C*, **111**(11), 4087–4093.

Ali B., Huang C.R., Qi Z.Y., Ali S., Daud M.K., Geng X.X. and Zhou W.J. (2013). 5-Aminolevulinic acid ameliorates cadmium-induced morphological, biochemical, and ultrastructural changes in seedlings of oilseed rape, *Environmental Science and Pollution Research*, **20**, 7256–7267.

Al-Swadi H.A., Usman A.R., Al-Farraj A.S., Al-Wabel M.I., Ahmad M. and Al-Faraj A. (2022). Sources toxicity potential, and human health risk assessment of heavy metals-laden soil and dust of urban and suburban areas as affected by industrial and mining activities, *Scientific Reports*, **12**(1), 8972.

Al-Wabel M.I., Usman A.R., El-Naggar A.H., Aly A.A., Ibrahim H.M., Elmaghraby S. and Al-Omran A. (2015). Conocarpus biochar as a soil amendment for reducing heavy metal availability and uptake by maize plants, *Saudi journal of biological sciences*, **22**(4), 503–511.

Baragaño D., Forján R., Álvarez N., Gallego J.R. and González A. (2022). Zero valent iron nanoparticles and organic fertilizer assisted phytoremediation in a mining soil: Arsenic and mercury accumulation and effects on the antioxidative system of Medicago sativa L, *Journal of Hazardous Materials*, **433**, 128748.

Bhowmick S., Chakraborty S. Mondal P. Van Renterghem W. Van den Berghe S Roman-Ross G. Chatterjee D. and Iglesias M. (2014). Montmorillonite-supported nanoscale zero-valent iron for removal of arsenic from aqueous solution: kinetics and mechanism *Chemical Engineering Journal.*, **243**, 14–23.

Brasili E., Bavasso I., Petruccelli V., Vilardi G., Valletta A., Dal Bosco C. and Di Palma L. (2020). Remediation of hexavalent chromium contaminated water through zero-valent iron nanoparticles and effects on tomato plant growth performance, *Scientific reports*, **10**(1), 1920.

Chen L., Tang M., Chen C., Chen M., Luo K., Xu J. and Wu F. (2017). Efficient bacterial inactivation by transition metal catalyzed auto-oxidation of sulfite, *Environmental Science and Technology*, **51**(21), 12663–12671.

Chen, X. L., Li, F., Xie, X. J., Li, Z. and Chen, L. (2019). Nanoscale zero-valent iron and chitosan functionalized Eichhornia crassipes biochar for efficient hexavalent chromium removal, *International Journal of Environmental Research and Public Health*, **16**(17), 3046.

Cui X., Hou D., Tang Y., Liu M., Qie H., Qian T. and Xu X. (2023). Effects of the application of nanoscale zero-valent iron on plants: Meta-analysis, mechanism, and prospects, *Science of The Total Environment*, 165873.

del Real A.P., Gonzalo P.G., Rodríguez A.G., Lobo M.C. and Sanz A.P. (2013). Effect of genotype, Cr (III) and Cr (VI) on plant growth and micronutrient status in Silene vulgaris (Moench), *Spanish Journal of Agricultural Research*, **11**(3), 685–694.

Deon F., van Ruitenbeek F., van der Werff H., van der Meijde M. and Marcatelli C. (2022). Detection of interlayered Illite/smectite clay minerals with XRD, SEM analyses and reflectance spectroscopy, *Sensors*, **22**(9), 3602.

Dong H., Zhao F., Zeng G., Tang L., Fan C., Zhang L. and Wu Y. (2016). Aging study on carboxymethyl cellulose-coated zero-

valent iron nanoparticles in water: chemical transformation and structural evolution, *Journal of hazardous materials*, **312**, 234–242.

Erskine R.H., Sherrod L.A. and Green T.R. (2017). Measuring and mapping patterns of soil erosion and deposition related to soil carbonate concentrations under agricultural management. JoVE (*Journal of Visualized Experiments*), (127), e56064.

Gil-Díaz M., Pinilla P., Alonso J. and Lobo M.C. (2017). Viability of a nanoremediation process in single or multi-metal (loid) contaminated soils, *Journal of hazardous materials*, **321**, 812–819.

Gill R.A., Hu X.Q., Ali B., Yang C., Shou J.Y., Wu Y.Y. and Zhou W.J. (2014). Genotypic variation of the responses to chromium toxicity in four oilseed rape cultivars, *Biologia plantarum*, **58**(3), 539–550.

Gu M., Farooq U., Lu S., Zhang X., Qiu Z. and Sui Q. (2018). Degradation of trichloroethylene in aqueous solution by rGO supported nZVI catalyst under several oxic environments, *Journal of hazardous materials*, **349**, 35–44.

Gupta U.C. and Kalra Y.P. (2006). Residual effect of copper and zinc from fertilizers on plant concentration, phytotoxicity, and crop yield response, *Communications in soil science and plant analysis,* **37**(15–20), 2505–2511.

Hasan M.S., Geza M., Vasquez R., Chilkoor G. and Gadhamshetty V. (2020). Enhanced heavy metal removal from synthetic stormwater using nanoscale zerovalent iron–modified biochar. Water, Air, & Soil Pollution, **231**, 1–15.

Hossner L.R. (1996). Dissolution for total elemental analysis, *Methods of soil analysis: part 3 chemical methods,* **5**, 49–64.

Ibrahim H.M., Awad M., Al-Farraj A.S. and Al-Turki A.M. (2019). Effect of flow rate and particle concentration on the transport and deposition of bare and stabilized zero-valent iron nanoparticles in sandy soil, *Sustainability*, **11**(23), 6608.

Jawed A., Golder A.K. and Pandey L.M. (2023). Synthesis of iron oxide nanoparticles mediated by Camellia sinensis var. Assamica for Cr (VI) adsorption and detoxification, *Bioresource Technology*, **376**, 128816.

Jawed A., Saxena V. and Pandey L.M. (2020). Engineered nanomaterials and their surface functionalization for the removal of heavy metals: A review. *Journal of Water Process Engineering*, **33**, 101009.

Jia Z., Li S. and Wang L. (2018). Assessment of soil heavy metals for eco-environment and human health in a rapidly urbanization area of the upper Yangtze Basin, *Scientific Reports*, **8**(1):3256.

Karabelli D., Üzüm C., Shahwan T., Eroglu A.E., Scott T.B., Hallam K.R., and Lieberwirth I. (2008). Batch removal of aqueous Cu^{2+} ions using nanoparticles of zero-valent iron: a study of the capacity and mechanism of uptake, *Industrial and Engineering Chemistry Research*, **47**(14), 4758-4764.

Li J., Zhang X., Sun Y., Liang L., Pan B., Zhang W., and Guan X. (2017). Advances in sulfidation of zerovalent iron for water decontamination, *Environmental science and technology*, **51**(23), 13533–13544.

Li Y., Jin Z. and Li T. (2012). A novel and simple method to synthesize SiO_2-coated Fe nanocomposites with enhanced Cr (VI) removal under various experimental conditions, *Desalination*, **288**, 118–125.

Li Z., Liu D., Huang W., Wei X. and Huang, W. (2020). Biochar supported CuO composites used as an efficient peroxymonosulfate activator for highly saline organic wastewater treatment, *Science of the Total Environment,* **721**, 137764.

Lin Y.H., Tseng H.H., Wey M. Y. and Lin, M.D. (2010). Characteristics of two types of stabilized nano zero-valent iron and transport in porous media, *Science of the Total Environment*, **408**(10), 2260–2267.

Liu Z., Zhang F.S. and Wu J. (2010). Characterization and application of chars produced from pinewood pyrolysis and hydrothermal treatment, *Fuel*, **89**(2), 510–514.

Lu H., Li Z., Fu S., Mendez A., Gasco G. and Paz-Ferreiro J. (2014). Can biochar and phytoextractors be jointly used for cadmium remediation?, *PLoS One*, 9(**4**), e95218.

Lyu H., Gao B., He F., Zimmerman A.R., Ding C., Huang H. and Tang J. (2018). Effects of ball milling on the physicochemical and sorptive properties of biochar: Experimental observations and governing mechanisms, *Environmental Pollution*, **233**, 54–63.

Ma X., Gurung A. and Deng Y. (2013). Phytotoxicity and uptake of nanoscale zero-valent iron (nZVI) by two plant species, *Science of the total environment*, **443**, 844-849.

Mandal S., Pu S., Shangguan L., Liu S., Ma H., Adhikari S. and Hou, D. (2020). Synergistic construction of green tea biochar supported nZVI for immobilization of lead in soil: A mechanistic investigation, *Environment international*, **135**, 105374.

Mwendwa S. (2022). Revisiting soil texture analysis: Practices towards a more accurate Bouyoucos method. *Heliyon*, **8**(5).

Mylavarapu R., Sikora F.J. and Moore K.P. (2014). Walkley-Black Method. Soil test methods from the Southeastern United States, **158**.

Němeček J., Lhotský O., & Cajthaml T. (2014). Nanoscale zero-valent iron application for in situ reduction of hexavalent chromium and its effects on indigenous microorganism populations. *Science of the Total Environment*, **485**, 739–747.

Premarathna K.S.D., Rajapaksha A. U., Adassoriya N., Sarkar B., Sirimuthu N.M., Cooray A. and Vithanage M. (2019). Clay-biochar composites for sorptive removal of tetracycline antibiotic in aqueous media, *Journal of environmental management*, **238**, 315–322.

Qian L., Shang X., Zhang B., Zhang W., Su A., Chen Y., and Chen M. (2019). Enhanced removal of Cr (VI) by silicon rich biochar-supported nanoscale zero-valent iron. *Chemosphere*, **215**, 739–745.

Rajkovich S., Enders A., Hanley K., Hyland C., Zimmerman A.R. and Lehmann J. (2012). Corn growth and nitrogen nutrition after additions of biochars with varying properties to a temperate soil, *Biology and Fertility of Soils*, **48**, 271–284.

Ren J., Mi X. and Tao L. (2021). Stabilization of cadmium in polluted soil using palygorskite-coated nanoscale zero-valent iron, *Journal of Soils and Sediments*, **21**, 1001–1009.

Shu Y., Ji B., Cui B., Shi Y., Wang J., H, M. and Guo, D. (2020). Almond shell-derived, biochar-supported, nano-zero-valent iron composite for aqueous hexavalent chromium removal: performance and mechanisms, *Nanomaterials*, **10**(2), 198.

SPSS. (2012). IBM SPSS statistics version 21. Boston, Mass: *International Business Machines Corp*.

Usman A.R., Sallam A.S., Al-Omran A., El-Naggar A.H., Alenazi K.K., Nadeem M. and Al-Wabel M.I. (2013). Chemically

modified biochar produced from conocarpus wastes: an efficient sorbent for Fe (II) removal from acidic aqueous solutions, *Adsorption Science and Technology*, **31**(7), 625–640.

Usman A.R.A. and Mohamed H.M. (2009). Effect of microbial inoculation and EDTA on the uptake and translocation of heavy metal by corn and sunflower, *Chemosphere*, **76**(7), 893–899.

Usman, A.R. A. and H.M. Mohamed. 2009. Effect of microbial inoculation and EDTA on the uptake and translocation of heavy metal by corn and sunflower. *Chemosphere*. **76**: 893–899.

Üzüm Ç., Shahwan T., Eroğlu A.E., Hallam K.R., Scott T.B. and Lieberwirth I. (2009). Synthesis and characterization of kaolinite-supported zero-valent iron nanoparticles and their application for the removal of aqueous Cu2+ and Co^{2+} ions, *Applied clay science*, **43**(2), 172–181.

Wang S., Gao B., Li Y., Creamer A.E. and He F. (2017). Adsorptive removal of arsenate from aqueous solutions by biochar supported zero-valent iron nanocomposite: batch and continuous flow tests, *Journal of hazardous materials*, **322**, 172–181.

Wang X., Wang A., Ma J. and Fu M. (2017). Facile green synthesis of functional nanoscale zero-valent iron and studies of its activity toward ultrasound-enhanced decolorization of cationic dyes, *Chemosphere*, **166**, 80–88.

Wang Y., Wang H.S., Tang C.S., Gu K. and Shi B. (2019). Remediation of heavy-metal-contaminated soils by biochar: a review, *Environmental Geotechnics*, **9**(3), 135–148.

Wei D., Li B., Luo L., Zheng Y., Huang L., Zhang J. and Huang H. (2020). Simultaneous adsorption and oxidation of antimonite onto nano zero-valent iron sludge-based biochar: Indispensable role of reactive oxygen species and redox-active moieties, *Journal of hazardous materials*, **391**, 122057.

Yan W., Lien H.L., Koel B.E. and Zhang W.X. (2013). Iron nanoparticles for environmental clean-up: recent developments and future outlook, *Environmental Science*, **15**(1), 63–77.

Yang F., Zhang S., Sun Y., Cheng K., Li J. and Tsang D.C. (2018). Fabrication and characterization of hydrophilic corn stalk biochar-supported nanoscale zero-valent iron composites for efficient metal removal, *Bioresource technology*, **265**, 490–497.

Yang F., Zhang S., Sun Y., Cheng K., Li J., and Tsang D. C. (2018). Fabrication and characterization of hydrophilic corn stalk biochar-supported nanoscale zero-valent iron composites for efficient metal removal. Bioresource technology, **265**, 490–497.

Yang Y., Guo J., and Zhiqiang H. (2013). Impact of nano zero valent iron (nZVI) on methanogenic activity and population dynamics in anaerobic digestion, *Water research,* **47**, 6790–6800.

Yang Y.M., Naseer M., Zhu Y., Zhu S.G., Wang S., Wang B.Z. and Xiong Y.C. (2022). Dual effects of nZVI on maize growth and water use are positively mediated by arbuscular mycorrhizal fungi via rhizosphere interactions, *Environmental Pollution*, **308**, 119661.

Yang Y.M., Zhu Y., Naseer M., Wang Q., Li G., Tao H.Y. and Xiong Y.C. (2023). Rhizosphere effect of nanoscale zero-valent iron on mycorrhiza-dependent maize assimilation, *Plant, Cell & Environment*, **46**(1), 251–267.

Yuan Y., Chai L., Yang Z. and Yang W. (2017). Simultaneous immobilization of lead, cadmium, and arsenic in combined contaminated soil with iron hydroxyl phosphate, *Journal of Soils and Sediments*, **17**, 432–439.

Zacchini M., Pietrini F., Scarascia Mugnozza G., Iori V., Pietrosanti L. and Massacci A. (2009). Metal tolerance, accumulation and translocation in poplar and willow clones treated with cadmium in hydroponics, *Water, Air, and Soil Pollution*, **197**, 23–34.

Zhang B. and Wang D. (2019b). Preparation of biomass activated carbon supported nanoscale zero-valent iron (nZVI) and its application in decolorization of methyl orange from aqueous solution, *Water,* **11**(8), 1671.

Zhang D. and Ding A. (2019). Effects of passivating agents on the availability of Cd and Pb and microbial community function in a contaminated acidic soil, *Bulletin of environmental contamination and toxicology*, **103**, 98–105.

Zhang D., Shen J., Shi H., Su G., Jiang X., Li J. and Wang L. (2019). Substantially enhanced anaerobic reduction of nitrobenzene by biochar stabilized sulfide-modified nanoscale zero-valent iron: Process and mechanisms, *Environment international*, **131**, 105020.

Zhao L., Zhao Y., Yang B. and Teng H. (2019). Application of carboxymethyl cellulose–stabilized sulfidated nano zerovalent iron for removal of Cr (VI) in simulated groundwater, *Water, Air, & Soil Pollution*, **230**, 1–14.

Zhu Y., Li H., Zhang G., Meng F., Li L. and Wu S. (2018). Removal of hexavalent chromium from aqueous solution by different surface-modified biochars: Acid washing, nanoscale zero-valent iron and ferric iron loading, *Bioresource Technology*, **261**, 142–150.

Zhuang P., Yang Q.W., Wang H.B. and Shu W.S. (2007). Phytoextraction of heavy metals by eight plant species in the field, *Water, Air, and Soil Pollution*, **184**, 235–242.

Zou Y., Wang X., Khan A., Wang P., Liu Y., Alsaedi A. and Wang X. (2016). Environmental remediation and application of nanoscale zero-valent iron and its composites for the removal of heavy metal ions: a review, *Environmental science & technology*, **50**(14), 7290–7304.